NeuroImage: Clinical 20 (2018) 1246–1254

Contents lists available at ScienceDirect

NeuroImage: Clinical

journal homepage: www.elsevier.com/locate/ynicl

Distinct cortical responses evoked by electrical stimulation of the thalamic ventral intermediate nucleus and of the subthalamic nucleus

Hartmann C.J.[a,b,*,1], Hirschmann J.[b,1], Vesper J.[c], Wojtecki L.[a,b], Butz M.[b], Schnitzler A.[a,b]

[a] Department of Neurology, Medical Faculty, Heinrich-Heine University Düsseldorf, Moorenstrasse 5, 40225 Düsseldorf, Germany
[b] Institute of Clinical Neuroscience and Medical Psychology, Medical Faculty, Heinrich-Heine University Düsseldorf, Moorenstrasse 5, 40225 Düsseldorf, Germany
[c] Department of Neurosurgery, Medical Faculty, Heinrich-Heine University Düsseldorf, Moorenstrasse 5, 40225 Düsseldorf, Germany

ARTICLE INFO

Keywords:
Deep brain stimulation
Cortical responses
Magnetoencephalography

ABSTRACT

Objective: To investigate the spatial and temporal pattern of cortical responses evoked by deep brain stimulation (DBS) of the subthalamic nucleus (STN) and ventral intermediate nucleus of the thalamus (VIM).
Methods: We investigated 7 patients suffering from Essential tremor (ET) and 7 patients with Parkinson's Disease (PD) following the implantation of DBS electrodes (VIM for ET patients, STN for PD patients). Magnetoencephalography (MEG) was used to record cortical responses evoked by electric stimuli that were applied via the DBS electrode in trains of 5 Hz. Dipole fitting was applied to reconstruct the origin of evoked responses.
Results: Both VIM and STN DBS led to short latency cortical responses at about 1 ms. The pattern of medium and long latency cortical responses following VIM DBS consisted of peaks at 13, 40, 77, and 116 ms. The associated equivalent dipoles were localized within the central sulcus, 3 patients showed an additional response in the cerebellum at 56 ms. STN DBS evoked cortical responses peaking at 4 ms, 11 ms, and 27 ms, respectively. While most dipoles were localized in the pre- or postcentral gyrus, the distribution was less homogenous compared to VIM stimulation and partially included prefrontal brain areas.
Conclusion: MEG enables localization of cortical responses evoked by DBS of the VIM and the STN, especially in the sensorimotor cortex. Short latency responses of 1 ms suggest cortical modulation which bypasses synaptic transmission, i.e. antidromic activation of corticofugal fiber pathways.

1. Introduction

Deep brain stimulation (DBS) is an established therapy for patients with advanced movement disorders like Parkinson's disease (PD) or Essential tremor (ET) (Lozano and Lipsman, 2013). Even though the mechanisms underlying DBS are still not completely understood, evidence grows that the associated modulation of cortical activity is crucial for its beneficial effects (Lozano and Lipsman, 2013). In particular, a current hypothesis for the mechanisms underlying effective DBS is the disruption of pathologic oscillatory activity.

PD is associated with increased synchronized activity especially in the beta frequency band within a brain network consisting of both cortical regions and the basal ganglia. Various studies could demonstrate the ability of DBS to modulate the temporal pattern in this network (Meissner et al., 2005; de Hemptinne et al., 2015; Oswal et al., 2016). With regard to ET, there is evidence for oscillatory interactions within a network consisting of cortical motor areas, thalamus, brainstem, and the cerebellum (Schnitzler et al., 2009). Previous studies showed that thalamic DBS is able to reduce pathological oscillatory activity in the theta frequency range (Connolly et al., 2012; Kane et al., 2009; Neely et al., 2014). The observation that motor cortex stimulation may alleviate PD and ET symptoms (Bentivoglio et al., 2012; Drouot et al., 2004; Moro et al., 2011) indicates that the cerebral cortex contributes to the therapeutic benefit of DBS.

Previous studies recorded cortical potentials evoked by electrical stimuli applied via the DBS electrodes to functionally investigate the neuronal network affected by DBS and its influence on cortical excitability. In particular, the detection of short latency responses complies with the hypothesis that antidromic activation of corticofugal fibers during STN stimulation may modulate cortical activity (Ashby et al.,

* Corresponding author at: Heinrich-Heine-University Düsseldorf, Department of Neurology, Moorenstrasse 5, 40225 Düsseldorf, Germany.
E-mail addresses: Christian.Hartmann@med.uni-duesseldorf.de (C.J. Hartmann), Jan.Hirschmann@med.uni-duesseldorf.de (J. Hirschmann), Jan.Vesper@med.uni-duesseldorf.de (J. Vesper), Lars.Wojtecki@med.uni-duesseldorf.de (L. Wojtecki), Markus.Butz@med.uni-duesseldorf.de (M. Butz), SchnitzA@med.uni-duesseldorf.de (A. Schnitzler).
[1] Equally regarded as first authors.

https://doi.org/10.1016/j.nicl.2018.11.001
Received 11 May 2018; Received in revised form 27 October 2018; Accepted 2 November 2018
Available online 03 November 2018

2001; Baker et al., 2002; MacKinnon et al., 2005; Walker et al., 2012a; Walker et al., 2012b). This notion tallies with animal studies (Li et al., 2007; Dejean et al., 2009; Gradinaru et al., 2009). Moreover, Whitmer et al. observed that STN DBS induced suppression of pathologic beta synchronization predominantly at the origin of the hyperdirect pathway, underlining the hypothesis of a link between antidromic cortical modulation (via the hyperdirect pathway) and the suppression of pathological oscillatory activity (Whitmer et al., 2012).

In order to more precisely identify the spatiotemporal patterns of cortical activations of STN and VIM stimulation, we used magnetoencephalography (MEG) to record evoked fields (EF) following electrical stimuli unilaterally administrated via a DBS electrode.

2. Patients and methods

2.1. Patients

The procedure of recording STN-LFP and MEG data in patients after electrode implantation and during external DBS was approved by the local ethics committee (study number 3209). According to the guidelines for good clinical practice and the declaration of Helsinki, patients were informed about the procedure, and gave prior written informed consent to participate in this study. We recruited 9 patients suffering from ET and 11 PD patients. 2 ET and 4 PD patients were excluded from analysis (see below). Patient data are provided in Table 1.

2.2. Surgery for DBS

Oral disease-related medication was withdrawn ≥12 h prior to surgery. Instead, PD patients received a continuous subcutaneous infusion of apomorphine to prevent severe hypokinesia. This treatment was stopped 1 h prior to surgery in order to ensure that both PD and ET patients presented symptoms that could be clinically investigated during surgery. The target location for DBS was derived from Schaltenbrand–Wahren atlas coordinates, using stereotactic cranial computer tomography (CT) and high resolution T1-weighted magnetic resonance imaging (MR, MP-Rage, slice thickness 1 mm). During DBS surgery, a multi-channel array (Ben-Gun) was used for micro-electrode recording. Up to five microelectrodes were forwarded (2 mm separation) anterior, posterior, medial, and lateral to a central microelectrode (INOMED Inc., Tenningen, Germany) to confirm the target area for DBS electrode placement (electrode model 3389 for PD patients and model 3387 for ET patients, Medtronic Corporation, Minneapolis, MN, USA). The decision for the final electrode placement was based on multi-unit activity and the clinical profile of test stimulation effects. Finally, the leads of the intracranial electrodes were externalized with custom-made non-ferromagnetic extension cables provided by the manufacturer for connecting an external amplifier. The pulse generator was implanted in a second surgery following MEG measurements.

2.3. Data acquisition

All recordings were performed with a 306-channel, whole-head MEG system (Elekta Oy, Helsinki, Finland) the day after electrode implantation. The sampling rate was 5 kHz. Patients did not receive disease-related medication at least 12 h prior to MEG recording. To verify the OFF state and to quantify the influence of presumably confounding factors like the stun effect, the MDS-UPDRS III was evaluated by an experienced neurologist for each PD patient. Before a patient underwent external stimulation (OSIRIS cortical stimulator, INOMED GmbH, Tenningen, Germany), all electrode impedances were checked. Only contacts with an impedance ≤2 kΩ were considered for stimulation. If impedances permitted, the second lowermost and the uppermost contacts of the electrode contralateral to the more affected body side were selected, since the second lowermost contact was typically seeded at the initially planned target height as specified by stereotactic planning. In some cases, these contacts could not be used due to high impedance. In this case, the lowermost and second uppermost contacts were used for stimulation, i.e. the distance between contacts remained the same but the contact pair was shifted in the ventral direction by one contact. To evaluate EF, a stimulation frequency of 5 Hz was applied, the pulse duration was kept constant at 60 μs.

ET patients underwent a series of 5 Hz stimulation epochs with stepwise increase of the amplitude by 0.5 mA from 0 mA up to 3.5 mA. The stimulation epochs lasted 30 s and were interposed by pauses of 10 s. For this study, we considered intensities between 1.5 and 3.5 mA (please refer to Fig. 2). The mean number of stimuli for a single patient was 1160 (range 900–1500). EF were normalized to individual baseline

Table 1
Pertinent data of patients (7 ET and PD patients) who were included for data analysis.

Pat.ID (ET/PD #)	Gender (m/f)	Age (years)	Side stimulated (VIM/STN left/right)	DBS amplitude (mA)	Anode coordinates (x/y/z)	Cathode coordinates (x/y/z)
ET 1	m	76	VIM left	3.5	−13/−15/4	−15/−13/9
ET 2	m	72	VIM right	3.5	13/−16/−3	16/−13/2
ET 3	m	67	VIM right	2.5	14/−16/−1	16/−13/4
ET 4	m	75	VIM left	3.0	−13/−18/0	−15/−17/6
ET 5	f	65	VIM right	3.0	12/−17/−3	14/−15/3
ET 6	m	49	VIM right	2.5	16/−17/−1	17/−13/3
ET 7	m	74	VIM right	2.5	14/−16/1	16/−13/6
Mean		67		2.9	13.6/−16.4/−0.4	15.6/−13.9/4.7
SD		10		0.4	1.3/1/2.4	1/1.6/2.4
PD 1	f	64	STN left	2.5	−11/−15/−6	−13/−13/−3
PD 2	f	66	STN left	3.0	−8/−18/−11	−9/−15/−8
PD 3	f	51	STN left	2.5	−11/−15/−5	−13/−13/−2
PD 4	f	60	STN right	2.5	12/−15/−7	14/−13/−4
PD 5	m	66	STN left	2.0	−11/−16/−5	−12/−14/−2
PD 6	m	65	STN left	2.5	−9/−14/−5	−11/−12/−2
PD 7	f	64	STN left	2.5	−9/−14/−7	−11/−12/−4
Mean		62		2.5	10.1/−15.3/−6.6	11.9/−13.1/−3.6
SD		5		0.3	1.5/1.4/2.1	1.7/1.1/2.1

DBS amplitude represents the highest current applied in ET patients and current applied in PD patients to evoke cortical responses. Anode and cathode coordinates specify the locations of respective electrode contacts after transformation to Montreal Neurological Institute space, as previously described (Hirschmann et al., 2013). The sign of the x-coordinates was flipped in patients who underwent left sided DBS before calculating the mean and standard deviation (SD). Abbreviations: *ET* = Essential Tremor, *PD* = Parkinson's Disease, *f* = female, *m* = male, *VIM* = ventral intermedius thalamic nucleus, *STN* = subthalamic nucleus, *DBS* = Deep Brain Stimulation.

levels −10 to −3 ms relative to stimulus onset. One ET patient was excluded from analysis because of artifacts and one patient was excluded due to a lack of sensor-level EF.

The EF of ET patients were compared to the EF of PD patients recorded in a later experiment using a different stimulation protocol. In this protocol, 30 s epochs of 130 Hz DBS were interleaved by 10 s epochs of 5 Hz DBS. Stimulation amplitude was constant throughout the measurement but varied across subjects due to individual safety limits. For the current analysis, we considered only the low frequency stimulation epochs. The mean number of stimuli for a single patient was 3179 (range 1747–4373). EF were normalized to individual baseline levels −10 to −3 ms relative to stimulus onset. Four patients were excluded from analysis because they lacked sensor-level EF.

In both patient groups, anode and cathode were switched after half of the pulses had been administered in order to minimize stimulation artifacts (Hirschmann et al., 2013).

2.4. Dipole fitting

To reconstruct the cortical current sources of the EF, individual, single-shell boundary element models based on anatomical MRI scans were constructed employing the Neuromag toolbox (MRI segmentation). The program XFit of the Neuromag toolbox was used to determine single equivalent current dipoles that explained the EF best. Dipole fitting was performed for a selection of sensors and time points. To minimize the influence of noise, EF were band-stop filtered before dipole fitting. EF evoked by VIM stimulation were low-pass filtered at 80 Hz and EF evoked by STN stimulation were band-pass filtered between 10 and 250 Hz. The filter's cut-off frequencies were determined after inspecting the unfiltered responses such that noise was reduced while the response pattern was preserved.

The gradiometer channel pair G_{max} with the maximal overall response was determined and selected. All immediate neighbors of G_{max} and their respective neighbors were added to the selection, provided that they showed the response as well.

After visual confirmation of a bipolar field pattern, a sequential fit was performed around each peak in G_{max}. For narrow peaks (first and second response in PD), fits were obtained from −1 to +1 ms in steps of 0.5 ms. For all other peaks, fits were obtained from −5 to +5 ms in steps of 1 ms.

If the maximal goodness-of-fit value in the series of fits was higher than 70%, the corresponding dipole was considered a localized source. In case none of the reconstructed dipoles provided a goodness-of-fit of > 70%, we tested whether artifact removal improved goodness-of-fit. The maxfilter application of the Neuromag software package was used to perform signal space separation (SSS) and the analysis was repeated (Taulu and Simola, 2006). We used the basic, not the temporal version of SSS with the default settings (inside extension order: 8, outside extension order: 3).

In order to identify additional responses which were not explained by the fitted dipoles, we added all localized sources to a multi-dipole model and fitted this model to the entire response pattern (all channels, all time points). The predicted pattern was visually compared to the true pattern. In case unexplained responses were observed, an additional dipole was fitted in the manner explained above.

2.5. Normalization of data for inter-individual comparison

Dipole coordinates were normalized to the Montreal Neurological Institute (MNI) 152 standard brain (MNI152-T1-1 mm), as provided by FMRIB Software Library v5.0 (FSL) (Jenkinson et al., 2012) using a symmetric normalization strategy with the ANTS software (Avants et al., 2011). Subsequently, the anatomical structure assigned to each dipole's location was identified using the “atlasquery” function in FSL. Primarily, the Harvard-Oxford Cortical Structural Atlas was utilized. If this atlas did not return a label for a given a dipole coordinate, the Harvard-Oxford Subcortical Structural Atlas was queried (for cerebellar dipoles: Cerebellar Atlas in MNI 152 space after normalization with FLIRT).

2.6. Assessment of dipole variability

To investigate whether the variability in dipole location was due to variability in stimulation site, we computed the distance between stimulation sites and the distance between dipole locations for each pair of patients and correlated these distances using Pearson's correlation coefficient. Stimulation site was defined as mean of the anode and cathode coordinates in MNI space.

2.7. Data quality

To provide an impression of data quality, we selected one representative ET and one PD patient, and for each of these patients, one sensor with a clear pulse artifact and data epochs with and without DBS (ET patient: 38 s DBS OFF, 29 s DBS ON at 2.5 mA; PD patient: 8.5 s DBS OFF, 9 s DBS ON at 2 mA). For the computation of power, data were cut in segments of 0.5 s length and 50% overlap, convolved with a Hanning taper and subjected to Fourier analysis.

3. Results

While DBS at 130 Hz can cause substantial artifacts in MEG data (Abbasi et al., 2016; Abbasi et al., 2018), bipolar DBS at 5 Hz was found to have only a minor impact on data quality in the cohorts studied here.

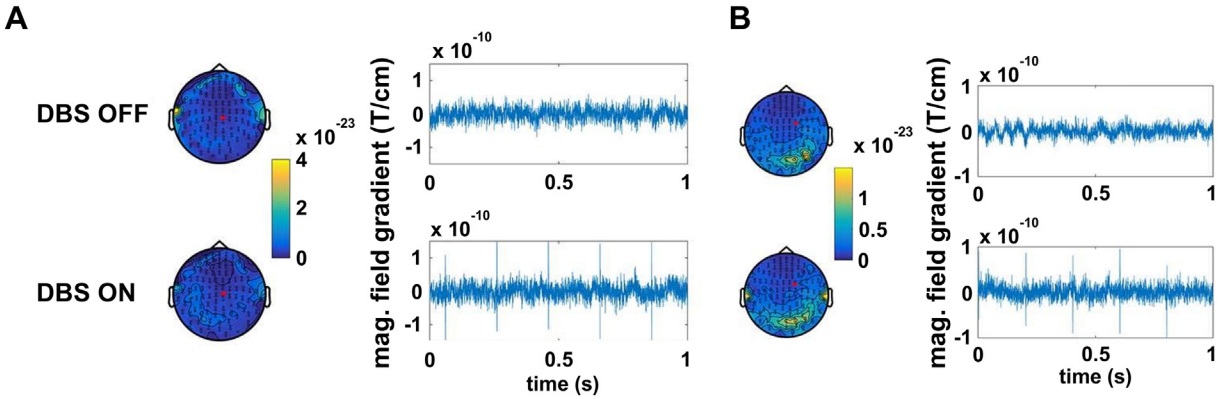

Fig. 1. Effects of deep brain stimulation (DBS) at 5 Hz on MEG signal quality. Upper row: DBS OFF. Lower row: DBS ON. A) Raw data sample (right) and topography of sensor power between 1 and 48 Hz (left) for ET patient ET 1. Power is color-coded (unit: T/cm^2). The red dot on the topographies marks the sensor selected for the raw data plots on the left. B) Same as A) for PD patient PD 3.

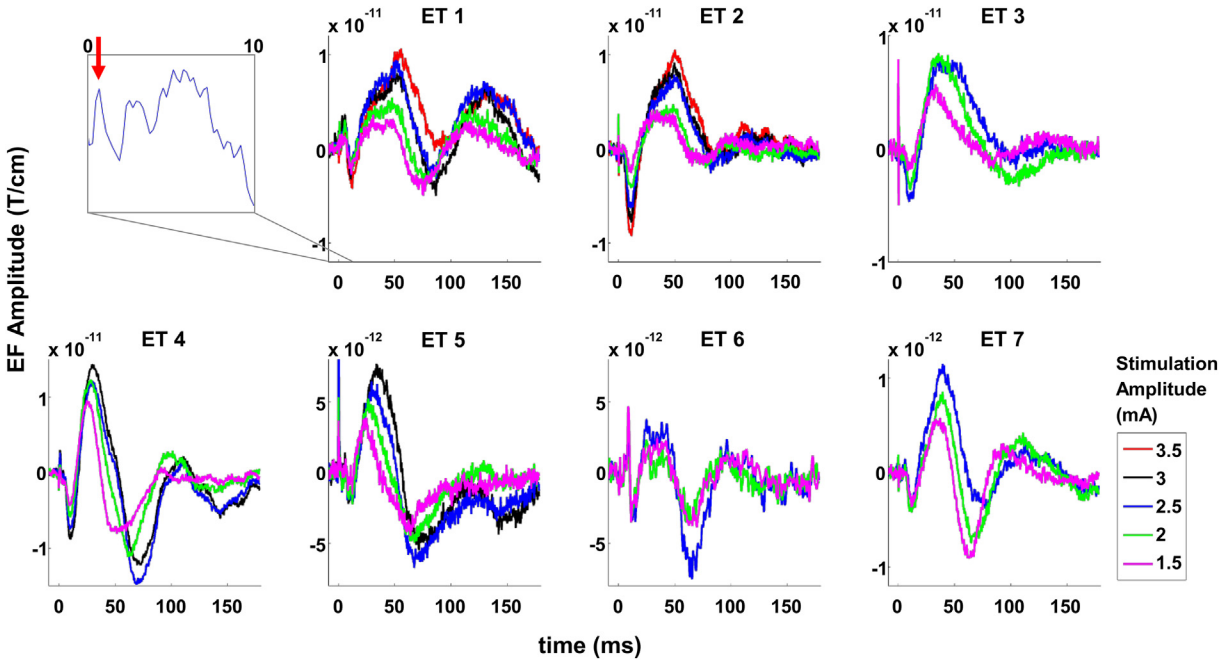

Fig. 2. Sensor level responses evoked by deep brain stimulation of the ventral intermediate nucleus of the thalamus in patients with essential tremor (unfiltered). Each sub-plot depicts the response of one patient, averaged over 3–5 channels located above sensorimotor cortex ipsilateral to stimulation. The inset shows an example of very early responses (< 10 ms) for patient ET 1; the red arrow indicates a peak at 1 ms. The peak amplitude of evoked fields increased with increasing stimulation amplitude (color-coded) in all patients under study.

Individual channels above the extension cable detected the DBS pulses but seemed unaffected otherwise (Fig. 1). Note that with respect to EF, the impact of artifacts is further reduced: artifacts not time-locked to DBS vanish through averaging and the pulse artifact itself is reduced by switching DBS polarity after half of the pulses have been administered (Walker et al., 2012a; Walker et al., 2012b).

3.1. Short latency responses

EF as early as 1 ms could be observed in 5 ET and 5 PD patients (see Fig. 2 inset), which will be called short latency responses in the following. Because the stimulation artifact could not be removed completely, these early responses could only be revealed in a limited number of cases.

3.2. Medium and long latency responses following VIM DBS

We observed highly consistent and reproducible EF in sensorimotor channels ipsilateral to stimulation in all patients (Fig. 1). These EF contained a first negative peakat 13 ms ± 1 ms), a first positive peak at 40 ms ± 9 ms, a second negative peak at 77 ms ± 13 ms, and a second positive peak at 116 ms ± 13 ms. Please note that the terms “positive” and “negative” are used here for ease of description. Polarity is contingent on the sensors' orientation relative to the current source.

The magnitude of these peaks increased with increasing stimulation amplitude. In all patients, a dipole could be adequately fitted to all or a subset of peaks. This dipole was located in or close to the central sulcus in all cases (mean goodness of fit 92 ± 9%, for details see Table 2). The direction of current flow alternated in a stereotypic fashion: anterior – posterior – anterior – posterior. Three subjects (ET 1, ET 2, and ET 7) showed an additional response in posterior sensors contralateral to stimulation. Corresponding sources were located in the contralateral cerebellar hemisphere (mean goodness of fit 87%, Fig. 3).

Across subjects, the distance between dipole locations was not correlated with the distance between stimulation sites, irrespective of the considered time (first negative peak: $r = 0.16$, $p = .66$; first positive peak: $r = -0.24$, $p = .51$; second negative peak: $r = 0.31$, $p = .39$; second positive peak: not enough data).

3.3. Medium latency responses following STN DBS

STN DBS also led to highly consistent EF in sensorimotor channels ipsilateral to stimulation (Fig. 4). However, the amplitudes were about an order of magnitude smaller than in ET. Moreover, EF were consistent only in the first 60 ms after the stimulation pulse, and highly variable afterwards. The pattern consisted of a first positive peak at 4 ms ± 0 ms, a second positive peak at 11 ± 1 ms, and a negative peak at 27 ± 6 ms. Table 3 summarizes the individual responses and the estimated dipole location.

Source locations are summarized in Fig. 5. In contrast to a very homogenous pattern in ET patients (Fig. 5A), the dipole location and orientation was more variable across PD patients. While most dipoles could be attributed to the pre- or postcentral gyrus, some of the dipoles were located in deeper brain areas such as cingulate cortex, especially those associated with the first positive peak (Fig. 5B).

Across subjects, the distance between dipole locations was correlated with the distance between stimulation sites for the first positive peak ($r = 0.54$, $p = .012$), but not for the second positive peak ($r = 0.05$, $p = .84$) nor for the first negative peak ($r = -0.01$, $p = .97$). In other words, patients with distant stimulation sites also had distant cortical responses at 4 ms.

4. Discussion

To our knowledge, this study is the first to localize cortical responses evoked by VIM and STN DBS using MEG. Our data demonstrate that both VIM and STN DBS lead to target-specific patterns of EF.

4.1. Peak latencies of EF

Our study revealed short latency responses in the majority of both VIM and STN DBS patients about 1 ms after the electric pulse was applied via the DBS electrode. Thus, we were able to substantiate the findings of previous EEG studies (Walker et al., 2012a, 2012b). Such a

Table 2
Sources of cortical responses evoked by VIM DBS in patients with essential tremor.

Subject ET	Peak type	Peak time (ms)	Fit time (ms)	x (mm)	y (mm)	z (mm)	Q (nAm)	g (%)	Location	P (%)	Orientation	SSS
ET 1	Neg1	13	14	−39	−15	36	17	91	PreCG	30	Anterior	y
ET 1	Pos1	52	53	−39	−24	38	23	98	PostCG	19	Posterior	y
ET 1	Neg2	83	83	−46	−12	48	14	90	PreCG	41	Anterior	y
ET 1	Pos2	131	134	−45	−3	42	11	78	PreCG	26	Posterior	y
ET 1	Add	65	66	54	−54	−44	9	87	CB Crus I		Dorsal	y
ET 2	Neg1	13	8	33	−31	30	35	95	CWM	100	Anterior	n
ET 2	Pos1	51	52	40	−23	31	43	95	CWM	100	Posterior	n
ET 2	Neg2	84	84	44	−23	38	16	94	PostCG	31	Anterior	n
ET 2	Pos2	111										n
ET 2	Add	40	38	−53	−68	−33	4	90	CB Crus I	57	Ventral	n
ET 3	Neg1	12	14	41	−9	28	24	97	PostCG	3	Anterior	n
ET 3	Pos1	36	45	52	−14	38	27	99	PostCG	43	Posterior	n
ET 3	Neg2	100										n
ET 3	Pos2	134										n
ET 4	Neg1	12	11	−45	−10	44	25	95	PreCG	43	Anterior	y
ET 4	Pos1	31	27	−45	−11	46	47	97	PreCG	40	Posterior	y
ET 4	Neg2	70	68	−50	−6	48	35	97	PreCG	60	Anterior	y
ET 4	Pos2	110	111	−46	−12	43	17	99	PreCG	44	Posterior	y
ET 5	Neg1	14										n
ET 5	Pos1	30	48	61	−3	40	8	79	PreCG	20	Posterior	n
ET 5	Neg2	69										n
ET 5	Pos2	118										n
ET 6	Neg1	14	19	38	−35	44	10	74	SMG PD	20	Anterior	n
ET 6	Pos1	38	42	34	−25	39	24	81	SMG AD	4	Posterior	n
ET 6	Neg2	65	72	38	−27	43	25	73	PostCG	39	Anterior	n
ET 6	Pos2	98										n
ET 7	Neg1	14	17	46	−11	35	24	96	PostCG	38	Anterior	n
ET 7	Pos1	41	43	45	−16	45	43	97	PostCG	40	Posterior	n
ET 7	Neg2	66	71	49	−13	47	35	97	PostCG	51	Anterior	n
ET 7	Pos2	113										n
ET 7	Add	62	67	−34	−42	−56	17	85	CB VIIIa	26	Dorsal/Lateral	n
Mean ± SD	Neg1	13 ± 1	14 ± 4	40 ± 5	−19 ± 11	36 ± 7	23 ± 9	92 ± 9				
	Pos1	40 ± 9	44 ± 9	45 ± 9	−17 ± 8	40 ± 5	31 ± 14	92 ± 9				
	Neg2	77 ± 13	76 ± 7	45 ± 5	−16 ± 9	45 ± 4	25 ± 10	90 ± 10				
	Pos2	116 ± 13	123 ± 16	46 ± 1	−8 ± 6	43 ± 1	14 ± 4	89 ± 15				
	Add	56 ± 24	57 ± 16	47 ± 11	−55 ± 13	−44 ± 12	10 ± 7	87 ± 2				

Peak type indicates the polarity of the sensor level peak. *Peak time* is the time of the peak in the filtered response and *Fit time* is the time with the best goodness-of-fit ± 5 ms from the peak. The values in the subsequent columns refer to the latter point in time. Dipole coordinates (*x*, *y*, *z*) are provided in Montreal Neurological Institute Space. The sign of the x-coordinates was flipped in patients who underwent left sided DBS before calculating the mean and standard deviation (SD). *Q* indicates the dipole moment and *g* indicates the goodness of fit. *P* is the probability that the dipole is truly located in the brain area given in the column *Location*. Only the label with maximum probability is listed. *SSS* indicates whether Signal Space Separation was applied. *CB* = cerebellum, *CWM* = cerebral white matter, *PostCG* = post-central gyrus, *PreCG* = precentral gyrus, *SMG AD* = supramarginal gyrus, anterior division, *SMG PD* = supra-marginal gyrus, posterior division.

short latency is very likely to result from antidromic activation of corticofugal fibers adjacent to the DBS electrode (Walker et al., 2012a, 2012b).

In VIM stimulation, we detected EF with a peak latency of 13 ms in all patients. This finding is compatible with the observations from an EEG study and most likely represents cortical responses after mono- and polysynaptic transmission (Walker et al., 2012b) via circuits that have yet to be revealed. EF following VIM stimulation with long latencies in the range of 77 and 116 ms, as observed in this study, have not been reported so far, but they resemble the responses evoked by transcranial stimulation of M1 (Bonato et al., 2006; Rogasch et al., 2013).

For STN-DBS, we observed a cortical response after 4 ms, which is similar to findings of earlier studies (Ashby et al., 2001; Walker et al., 2012a; Kuriakose et al., 2010) and compatible with monosynaptic orthodromic stimulation (Walker et al., 2012a; Nambu et al., 2000). Additionally, we detected a response 11 ms after the DBS pulse, similar to prior studies (Ashby et al., 2001; MacKinnon et al., 2005; Kuriakose et al., 2010), which is likely to represent poylsynaptic transmission. Further cortical responses occurred around 27 ms after STN stimulation. Two of our patients showed EF peaks at 21 ms, in agreement with previous studies (MacKinnon et al., 2005; Walker et al., 2012a; Kuriakose et al., 2010; Eusebio et al., 2009). The remaining five patients showed peaks between 26 and 36 ms after stimulation. Although these latencies are larger than reported in the aforementioned studies, they are in line with findings reported by Baker and colleagues (Baker et al., 2002), and similar to the results observed by Devergnas et al., who additionally showed that cortical responses evoked from pallidal stimulation occurred after about 25 ms, hence earlier than STN-evoked responses (Devergnas and Wichmann, 2011). This observation in turn leads to the assumption that medium latency effects due to STN stimulation may be driven either via direct stimulation of pallidothalamic fibers in the zona incerta and the fields of Forel or STN efferents to the pallidum, which propagate the signal via pallido-thalamo-cortical pathways.

Note that the variability of peak latencies is most likely caused by the variability of electrode positions: stimulation at the dorsal border of the STN would allow for activation of pallido-thalamic fibers whereas a more inferior stimulation in the core of the STN is more likely to stimulate STN efferents to the pallidum. In line with this assumption, the spatial variability of the response at 4 ms was related to the variability in stimulation site.

In summary, orthodromic cortical responses to STN DBS occured earlier (after 4 and 11 ms) than responses to VIM DBS (after 13, 40, 77 and 116 ms) suggesting that different neural pathways are involved in mediation of VIM DBS and STN DBS evoked responses.

4.2. Spatial representation of EF

Source localization of EF in VIM DBS revealed that most dipoles were located in or close to M1 and the primary sensory (S1) cortex,

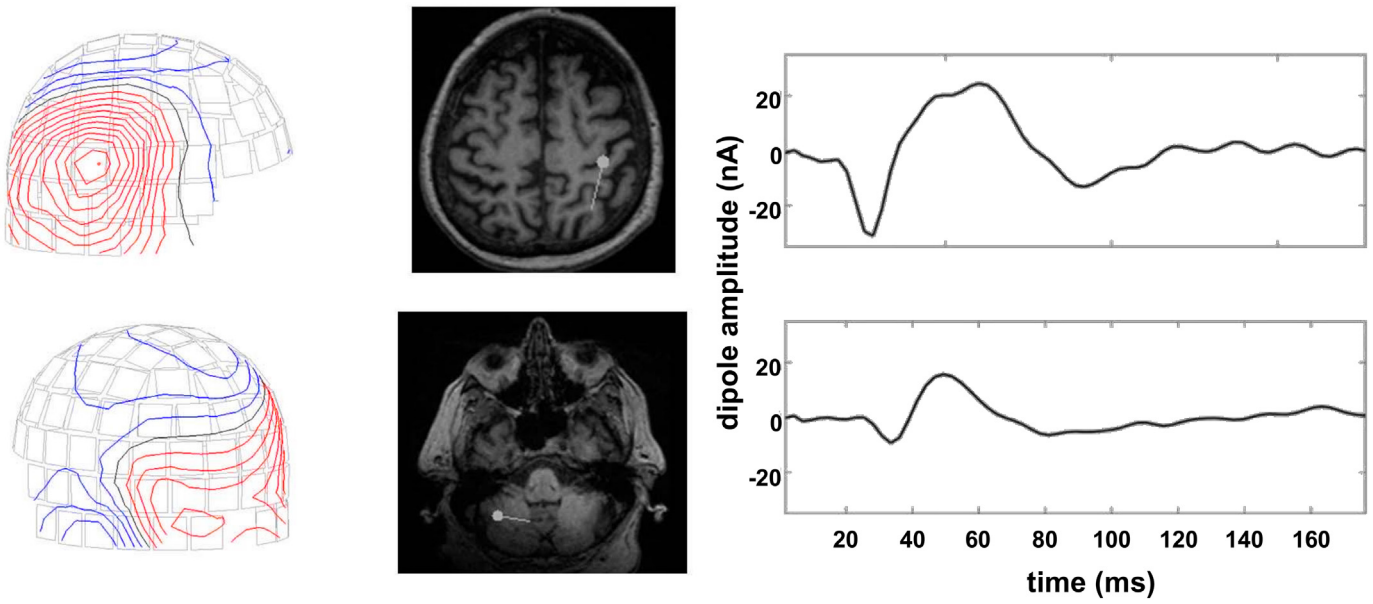

Fig. 3. Response localization in a patient with essential tremor (ET 2). The field topography (left column) is consistent with a central (upper row) and a cerebellar source (lower row). Deep brain stimulation was applied in the right thalamus. Contour plots show the spatial distribution of the magnetic field at 38 ms after the stimulation pulse. The middle column depicts the dipole localization at this time using a group of right sensorimotor channels and a group of left occipital channels, respectively. The right column shows dipole amplitude fits for the entire trial duration.

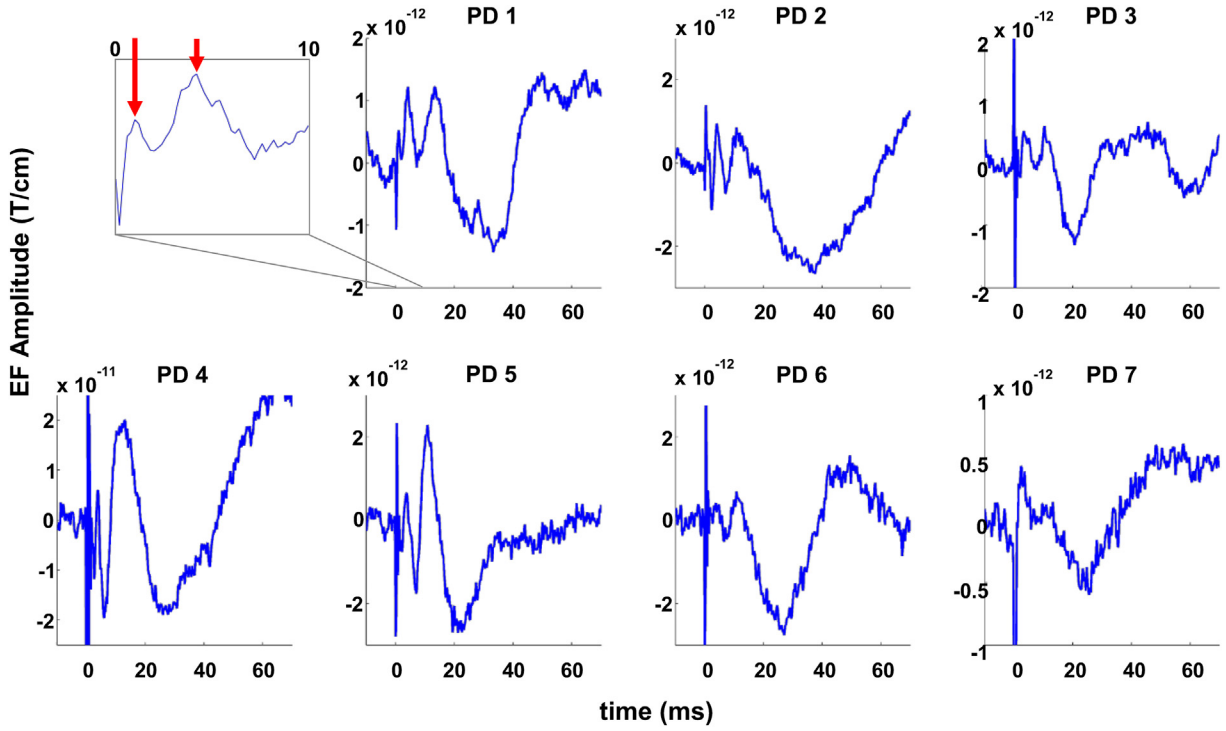

Fig. 4. Sensor level responses evoked by DBS of the subthalamic nucleus in PD patients (unfiltered). Each sub-plot depicts the response of one subject, averaged over 3–5 sensorimotor channels ipsilateral to stimulation. The inset shows an example of very early responses (< 10 ms) for patient PD 1, showing peaks at 1 and 4 ms, respectively (red arrows). Stimulation amplitude remained constant. The time axis is restricted to the first 60 ms, as subject-specific responses were consistent only within this period. Please note that the y axis scaling is generally smaller than in Fig. 2.

which is compatible with findings by Walker et al. (Walker et al., 2012b). In a subset of 3 ET patients, additional dipoles were localized in the cerebellum contralateral to stimulation.

VIM DBS is predominantly used to treat ET, whereas cerebellar dysfunction is considered a hallmark of the underlying pathology, as supported by imaging (Sharifi et al., 2014) and neuropathological studies (Louis, 2015). Functional imaging studies also suggest the involvement of the rolandic area in the pathophysiology of ET (Schnitzler et al., 2009; Connolly et al., 2012; Neely et al., 2015; Muthuraman et al., 2010), and recent studies identified a link between rolandic area and cerebellum by demonstrating an impairment of VIM-cortico-cerebellar pathways (Fang et al., 2015a, 2015b). Indeed, the targeting of VIM-cortico-cerebellar pathways has been proposed to optimize electrode placement (Sammartino et al., 2016; King et al.,

Table 3
Sources of cortical responses evoked by STN DBS in patients with Parkinson's disease.

Subject PD	Peak type	Peak time (ms)	Fit time (ms)	x (mm)	y (mm)	z (mm)	Q (nAm)	g (%)	Location	P (%)	Orientation	SSS
PD 1	Pos1	4	6	−13	−22	18	50	88	Thalamus	67	Ventral/lateral	y
PD 1	Pos2	13	10	−7	−25	47	13	93	PreCG	40	Lateral	y
PD 1	Neg1	33	18	−24	−25	56	7	93	PreCG	36	Anterior	y
PD 2	Pos1	4	6	−31	−15	42	13	93	PreCG	13	Anterior/ventral	y
PD 2	Pos2	11	14	−35	−12	46	10	97	PreCG	26	Anterior	y
PD 2	Neg1	36	43	−37	−14	48	10	97	PreCG	45	Posterior	y
PD 3	Pos1	4	7	−18	−19	37	10	95	PreCG	1	Lateral	y
PD 3	Pos2	11	14	1	45	24	10	86	PCG	70	Ventral/medial	y
PD 3	Neg1	21	22	−8	−21	54	12	98	PreCG	24	Medial/posterior	y
PD 4	Pos1	4	3	2	−51	20	59	80	Cin PD	43	Dorsal/lateral	y
PD 4	Pos2	12	12,5	43	−61	54	13	97	LOC	51	Anterior	y
PD 4	Neg1	26	24	28	−40	34	34	96	SPL	2	Posterior/medial	y
PD 5	Pos1	4	3,5	−13	−33	28	22	93	CWM	100	Anterior/lateral	y
PD 5	Pos2	11	9	−32	−30	50	9	97	PostGC	34	Anterior	y
PD 5	Neg1	21	24	−25	−27	48	14	99	PreCG	7	Posterior	y
PD 6	Pos1	4	4	7	−38	3	120	89	Cin PD	7	Dorsal	y
PD 6	Pos2	11	11	−51	−25	34	5	93	SMG AD	22	Anterior	y
PD 6	Neg1	27	26	−36	−18	20	19	98	COC	23	Posterior	y
PD 7	Pos1	4	6	−7	−11	25	18	88	CWM	54	Anterior	y
PD 7	Pos2	11	11	−55	9	39	1	74	PreCG	52	Ventral/anterior	y
PD 7	Neg1	26	29	−30	13	16	7	92	COC	2	Medial/anterior	y
Mean ± SD	Pos1	4 ± 0	5 ± 2	11 ± 12	−27 ± 14	25 ± 13	42 ± 40	90 ± 5				
	Pos2	11 ± 1	12 ± 2	32 ± 21	−14 ± 33	42 ± 11	9 ± 4	91 ± 8				
	Neg1	27 ± 6	27 ± 8	27 ± 10	−19 ± 16	40 ± 16	15 ± 9	96 ± 3				

Peak type indicates the direction of the sensor level peak. *Peak time* is the time of the peak in the filtered responses and *Fit time* is the time with the best goodness-of-fit ± 1 ms from the peak (± 5 ms for Neg1). The values in the subsequent columns refer to the latter point in time. Dipole coordinates (*x*, *y*, *z*) are provided in Montreal Neurological Institute Space. The sign of the x-coordinates was flipped in patients who underwent left sided DBS before calculating the mean and standard deviation (SD). *Q* indicates the dipole moment and *g* indicates the goodness of fit. *P* is the probability that the dipole is truly located in the brain area given in the column *Location*. Only the label with maximum probability is listed. *SSS* indicates whether Signal Space Separation was applied. *Cin PD* = cingulate, posterior division, *COC* = central opercular cortex, *CWM* = cerebral white matter, *LOC* = lateral occipital cortex, *PCG* = paracingulate gyrus, *PostCG* = postcentral gyrus, *PreCG* = precentral gyrus, *SMG AD* = supramarginal gyrus, anterior division, *SPL* = superior parietal lobule.

n.d.). A recent tractography study for VIM DBS in tremor patients suggests that clinical benefit is optimal when the active contact is placed in an area structurally connected to both ipsilateral primary motor cortex and contralateral cerebellum. (Akram et al., 2018). Given the lower chronaxies of axonal fibers compared to neural somata, spread of the electric field generated by DBS into white mater may facilitate generation and propagation of more action potentials than pure stimulation of thalamic nuclei. As such, it may also enhance the activation of cerebellar fiber pathways like the dentatorubrothalamic tract. We hypothesize that the active contact was closer to such fiber pathways in those three ET patients in our sample who showed cerebellar responses. Future studies may address the question whether the presence of cerebellar EF in VIM DBS is a predictor for good clinical outcome.

For STN DBS, M1 and S1 were the predominant sources of EF, which is in line with previous studies (Ashby et al., 2001; Baker et al., 2002; MacKinnon et al., 2005; Walker et al., 2012a; Kuriakose et al., 2010; Eusebio et al., 2009), and comparable to our findings in VIM DBS. Various studies have demonstrated functional connectivity between the STN and the sensorimotor cortex and premotor cortex in PD (Baudrexel et al., 2011; Hirschmann et al., 2011; Litvak et al., 2011), and modulation of the sensorimotor cortex was shown to be relevant for therapeutic effect of STN DBS in both animal and human studies (de Hemptinne et al., 2015; Li et al., 2007; Gradinaru et al., 2009; Abbasi et al., 2018; Luoma et al., 2018). Our study further supports the finding of previous studies that STN DBS influences additional targets to M1, especially the cingulate gyrus, which in turn may mediate non-motor effects of STN DBS (Knight et al., 2015). In this case, the observed pattern might relate to unwanted side-effects, as neuromodulation of the posterior cingulate due to STN DBS has been associated with apathy (Le Jeune et al., 2009) and impaired performance in random number generation and Go/NoGo tasks (Thobois et al., 2007; Ballanger et al., 2009).

In summary, we observed some differences in response location between STN and VIM stimulation: First, dipoles were less homogeneously distributed in STN DBS compared to VIM DBS. Second, VIM DBS evoked additional responses in the cerebellum, which were not observed for STN DBS. Despite these differences, however, both targets were found to modulate primarily sensorimotor cortex. Its predominant role is supported by the fact that not only deep brain stimulation, but also magnetic and electric stimulation of M1, the supplementary and premotor cortex have been shown to improve motor symptoms in movement disorders with and without clinical response to DBS (Priori and Lefaucheur, 2007; Kamble et al., 2014), even though, in DBS-responsive disorders, clinical benefit was less remarkable and less consistent compared to DBS.

4.3. Amplitudes of EF

EF following STN DBS were about an order of magnitude smaller, compared to VIM DBS. This finding may be caused by different cortical representations of activated fiber pathways, assuming more connected fibers between cortex and thalamus (cortico-thalamic and thalamo-cortical pathways) than between cortex and STN (hyperdirect pathway), hence leading to a higher cumulative effect on the cortical level. Another possible explanation for this finding is the usage of different electrode models for VIM and STN DBS. The centers of two adjacent contacts of the DBS electrode were separated by 2 mm for STN DBS and by 3 mm for VIM DBS. Since DBS was performed with a bipolar stimulation, the volume of tissue activated was presumably larger in ET patients than in PD patients, potentially leading to higher amplitudes of the EF.

Finally, we cannot exclude that the different paradigms contributed to the observed differences between ET and PD patients. It is possible, for example, that the 130 Hz train immediately preceding 5 Hz DBS in PD patients led to a reduction of EF amplitude in this group.

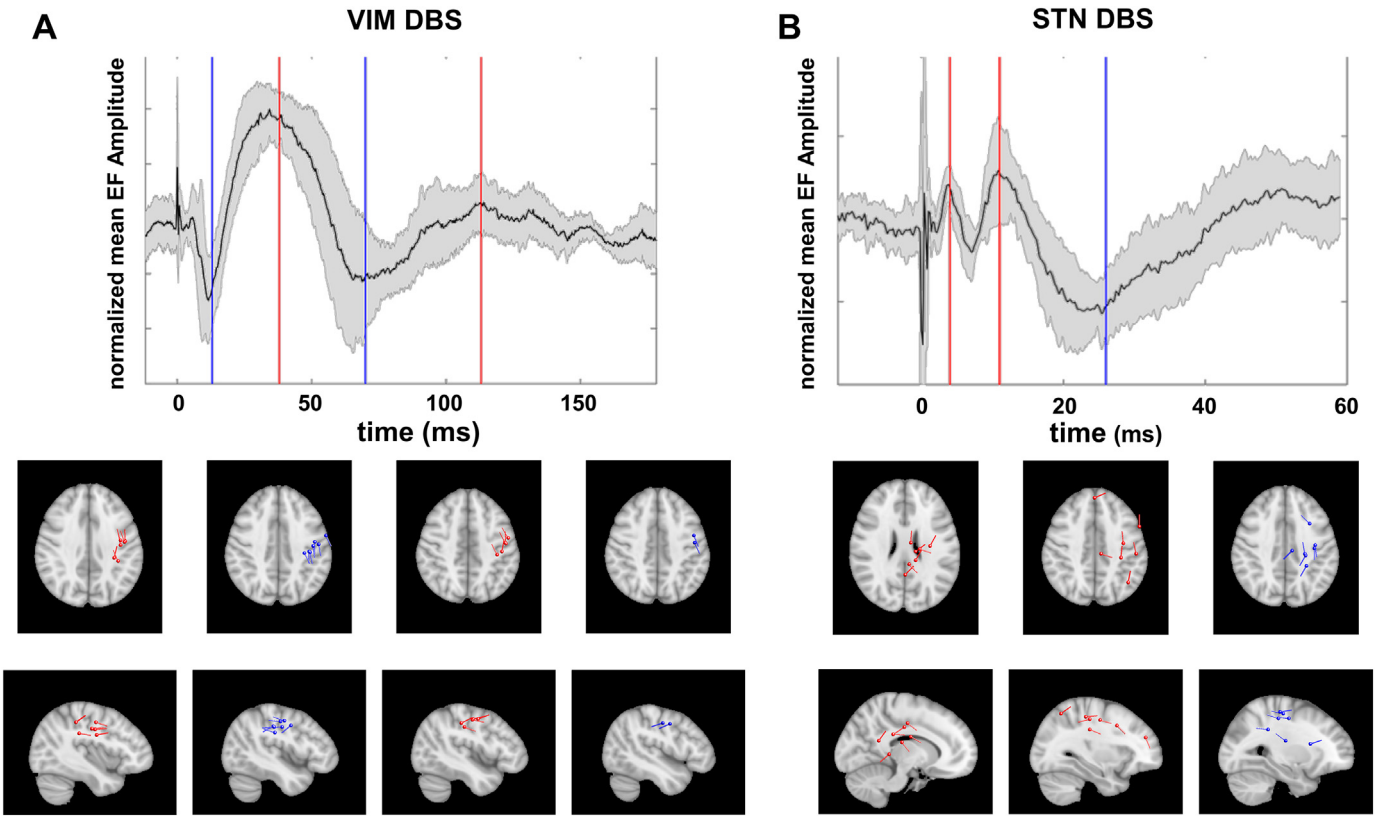

Fig. 5. Summary of source locations and waveforms. A) Responses to stimulation of the ventral intermediate nucleus of the thalamus in patients with Essential Tremor. B) Responses to stimulation of the subthalamic nucleus in patients with Parkinson's disease. The top panel depicts mean, z-transformed evoked responses on the sensor level. The shaded area marks the standard deviation and vertical lines indicate median peak times for upward (red) and downward deflections (blue). The lower panel shows the corresponding dipole locations in standard space (MNI152-T1-1 mm). To facilitate visualization, dipoles were projected onto the canonical plane that minimized squared distances. Dipole moments were set to unity and dipoles in the left hemisphere were mirrored across the mid-sagittal plane. (For interpretation of the references to color in this figure legend, the reader is referred to the web version of this article.)

4.4. Conclusion and outlook

Cortical responses evoked by VIM or STN DBS can be precisely described using MEG, with regard to both their spatial representation and their temporal dynamics. As such, this method complements currently existing techniques for combined analysis of DBS with MEG (Harmsen et al., 2018). The EF detected in our study were consistent among patients and demonstrated that both STN and VIM DBS primarily affect the sensorimotor region of the cortex. To delineate its relevance in the mediation of efficacious DBS, we suggest a comparison between efficacious and non-efficacious stimulation settings in future studies.

Detection of EF outside the sensorimotor region, as observed in our study, should be correlated with therapeutic and adverse effects of chronic DBS. In particular, the relevance of cerebellar fibers may be addressed for optimal tremor control and also for estimating the likelihood to develop (delayed) side effects like gait dysfunction (Reich et al., 2016).

For STN DBS patients, careful neuropsychological assessment in turn may help decide if modulation of prefrontal areas like the cingulate cortex, as observed in this study, is associated with non-motor side effects. Given the similarities of the EF found in this study with cortical responses evoked by transcranial stimulation, the simultaneous application of both techniques (DBS and transcranial stimulation) may help better characterizing the network effects of brain stimulation (Udupa et al., 2016).

Conflicts of interest

CJH, LW, JV, and AS received speaker/consultancy honoraria and/or grants by Medtronic, Abbott/St. Jude Medical, Boston Scientific and/or Inomed, companies that manufacture deep brain stimulations devices and/or intraoperative recording systems. JH and MB have no conflicts of interest to declare.

Acknowledgements

We would like to thank the patients for their participation in this study. Furthermore, we thank the people of Medtronic Neuromodulation (Dr. Ali Sarem-Aslani, Mr. Paul van Venrooij, and Mr. Andreas Rolf) for technical support. Additionally, we want to thank Nienke Hogenboom for her support. This study was supported by a grant of the Klinische Forschungskommission of the Heinrich-Heine-Universität Düsseldorf (55/2011).

References

Abbasi, O., Hirschmann, J., Schmitz, G., Schnitzler, A., Butz, M., 2016. Rejecting deep brain stimulation artefacts from MEG data using ICA and mutual information. J. Neurosci. Methods 268, 131–141.

Abbasi, O., Hirschmann, J., Storzer, L., Ozkurt, T.E., Elben, S., Vesper, J., et al., 2018. Unilateral deep brain stimulation suppresses alpha and beta oscillations in sensorimotor cortices. NeuroImage 174, 201–207.

Akram, H., Dayal, V., Mahlknecht, P., Georgiev, D., Hyam, J., Foltynie, T., et al., 2018. Connectivity derived thalamic segmentation in deep brain stimulation for tremor. NeuroImage Clin. 18, 130–142.

Ashby, P., Paradiso, G., Saint-Cyr, J.A., Chen, R., Lang, A.E., Lozano, A.M., 2001. Potentials recorded at the scalp by stimulation near the human subthalamic nucleus. Clin. Neurophysiol. 112 (3), 431–437.

Avants, B.B., Tustison, N.J., Song, G., Cook, P.A., Klein, A., Gee, J.C., 2011. A reproducible evaluation of ANTs similarity metric performance in brain image registration. NeuroImage 54 (3), 2033–2044.
Baker, K.B., Montgomery Jr., E.B., Rezai, A.R., Burgess, R., Luders, H.O., 2002. Subthalamic nucleus deep brain stimulus evoked potentials: physiological and therapeutic implications. Mov. Disord. 17 (5), 969–983.
Ballanger, B., van Eimeren, T., Moro, E., Lozano, A.M., Hamani, C., Boulinguez, P., et al., 2009. Stimulation of the subthalamic nucleus and impulsivity: release your horses. Ann. Neurol. 66 (6), 817–824.
Baudrexel, S., Witte, T., Seifried, C., von Wegner, F., Beissner, F., Klein, J.C., et al., 2011. Resting state fMRI reveals increased subthalamic nucleus-motor cortex connectivity in Parkinson's disease. NeuroImage 55 (4), 1728–1738.
Bentivoglio, A.R., Fasano, A., Piano, C., Soleti, F., Daniele, A., Zinno, M., et al., 2012. Unilateral extradural motor cortex stimulation is safe and improves Parkinson disease at 1 year. Neurosurgery 71 (4), 815–825.
Bonato, C., Miniussi, C., Rossini, P.M., 2006. Transcranial magnetic stimulation and cortical evoked potentials: a TMS/EEG co-registration study. Clin. Neurophysiol. 117 (8), 1699–1707.
Connolly, A.T., Bajwa, J.A., Johnson, M.D., 2012. Cortical magnetoencephalography of deep brain stimulation for the treatment of postural tremor. Brain Stimulation 5 (4), 616–624.
Dejean, C., Hyland, B., Arbuthnott, G., 2009. Cortical effects of subthalamic stimulation correlate with behavioral recovery from dopamine antagonist induced akinesia. Cereb. Cortex 19 (5), 1055–1063.
Devergnas, A., Wichmann, T., 2011. Cortical potentials evoked by deep brain stimulation in the subthalamic area. Front. Syst. Neurosci. 5, 30.
Drouot, X., Oshino, S., Jarraya, B., Besret, L., Kishima, H., Remy, P., et al., 2004. Functional recovery in a primate model of Parkinson's disease following motor cortex stimulation. Neuron 44 (5), 769–778.
Eusebio, A., Pogosyan, A., Wang, S., Averbeck, B., Gaynor, L.D., Cantiniaux, S., et al., 2009. Resonance in subthalamo-cortical circuits in Parkinson's disease. Brain 132, 2139–2150 Pt 8.
Fang, W., Chen, H., Wang, H., Zhang, H., Puneet, M., Liu, M., et al., 2015a. Essential tremor is associated with disruption of functional connectivity in the ventral intermediate Nucleus-Motor Cortex-Cerebellum circuit. Hum. Brain Mapp. 37 (1), 165–178.
Fang, W., Chen, H., Wang, H., Zhang, H., Liu, M., Puneet, M., et al., 2015b. Multiple resting-state networks are associated with tremors and cognitive features in essential tremor. Mov. Disord. 30 (14), 1926–1936.
Gradinaru, V., Mogri, M., Thompson, K.R., Henderson, J.M., Deisseroth, K., 2009. Optical deconstruction of parkinsonian neural circuitry. Science 324 (5925), 354–359.
Harmsen, I.E., Rowland, N.C., Wennberg, R.A., Lozano, A.M., 2018. Characterizing the effects of deep brain stimulation with magnetoencephalography: a review. Brain Stimul. 11 (3), 481–491.
de Hemptinne, C., Swann, N.C., Ostrem, J.L., Ryapolova-Webb, E.S., San Luciano, M., Galifianakis, N.B., et al., 2015. Therapeutic deep brain stimulation reduces cortical phase-amplitude coupling in Parkinson's disease. Nat. Neurosci. 18 (5), 779–786.
Hirschmann, J., Ozkurt, T.E., Butz, M., Homburger, M., Elben, S., Hartmann, C.J., et al., 2011. Distinct oscillatory STN-cortical loops revealed by simultaneous MEG and local field potential recordings in patients with Parkinson's disease. NeuroImage 55 (3), 1159–1168.
Hirschmann, J., Hartmann, C.J., Butz, M., Hoogenboom, N., Ozkurt, T.E., Elben, S., et al., 2013. A direct relationship between oscillatory subthalamic nucleus-cortex coupling and rest tremor in Parkinson's disease. Brain 136, 3659–3670 Pt 12.
Jenkinson, M., Beckmann, C.F., Behrens, T.E., Woolrich, M.W., Smith, S.M., 2012. Fsl. NeuroImage 62 (2), 782–790.
Kamble, N., Netravathi, M., Pal, P.K., 2014. Therapeutic applications of repetitive transcranial magnetic stimulation (rTMS) in movement disorders: a review. Parkinsonism Relat. Disord. 20 (7), 695–707.
Kane, A., Hutchison, W.D., Hodaie, M., Lozano, A.M., Dostrovsky, J.O., 2009. Enhanced synchronization of thalamic theta band local field potentials in patients with essential tremor. Exp. Neurol. 217 (1), 171–176.
King, N.K., Krishna, V., Basha, D., Elias, G., Sammartino, F., Hodaie, M., et al., 2016. Microelectrode recording findings within the tractography-defined ventral intermediate nucleus. J. Neurosurg. 1–7.
Knight, E.J., Testini, P., Min, H.K., Gibson, W.S., Gorny, K.R., Favazza, C.P., et al., 2015. Motor and nonmotor circuitry activation induced by subthalamic nucleus deep brain stimulation in patients with Parkinson disease: intraoperative functional magnetic resonance imaging for deep brain stimulation. Mayo Clin. Proc. 90 (6), 773–785.
Kuriakose, R., Saha, U., Castillo, G., Udupa, K., Ni, Z., Gunraj, C., et al., 2010. The nature and time course of cortical activation following subthalamic stimulation in Parkinson's disease. Cereb. Cortex 20 (8), 1926–1936.
Le Jeune, F., Drapier, D., Bourguignon, A., Peron, J., Mesbah, H., Drapier, S., et al., 2009. Subthalamic nucleus stimulation in Parkinson disease induces apathy: a PET study. Neurology 73 (21), 1746–1751.
Li, S., Arbuthnott, G.W., Jutras, M.J., Goldberg, J.A., Jaeger, D., 2007. Resonant antidromic cortical circuit activation as a consequence of high-frequency subthalamic deep-brain stimulation. J. Neurophysiol. 98 (6), 3525–3537.
Litvak, V., Jha, A., Eusebio, A., Oostenveld, R., Foltynie, T., Limousin, P., et al., 2011. Resting oscillatory cortico-subthalamic connectivity in patients with Parkinson's disease. Brain 134 (Pt 2), 359–374.
Louis, E.D., 2015. Linking essential tremor to the cerebellum: neuropathological evidence. Cerebellum 15 (3), 235–242.
Lozano, A.M., Lipsman, N., 2013. Probing and regulating dysfunctional circuits using deep brain stimulation. Neuron 77 (3), 406–424.
Luoma, J., Pekkonen, E., Airaksinen, K., Helle, L., Nurminen, J., Taulu, S., et al., 2018. Spontaneous sensorimotor cortical activity is suppressed by deep brain stimulation in patients with advanced Parkinson's disease. Neurosci. Lett. 683, 48–53.
MacKinnon, C.D., Webb, R.M., Silberstein, P., Tisch, S., Asselman, P., Limousin, P., et al., 2005. Stimulation through electrodes implanted near the subthalamic nucleus activates projections to motor areas of cerebral cortex in patients with Parkinson's disease. Eur. J. Neurosci. 21 (5), 1394–1402.
Meissner, W., Leblois, A., Hansel, D., Bioulac, B., Gross, C.E., Benazzouz, A., et al., 2005. Subthalamic high frequency stimulation resets subthalamic firing and reduces abnormal oscillations. Brain 128, 2372–2382 Pt 10.
Moro, E., Schwalb, J.M., Piboolnurak, P., Poon, Y.Y., Hamani, C., Hung, S.W., et al., 2011. Unilateral subdural motor cortex stimulation improves essential tremor but not Parkinson's disease. Brain 134, 2096–2105 Pt 7.
Muthuraman, M., Heute, U., Deuschl, G., Raethjen, J., 2010. The central oscillatory network of essential tremor. Conf. Proc. 2010, 154–157.
Nambu, A., Tokuno, H., Hamada, I., Kita, H., Imanishi, M., Akazawa, T., et al., 2000. Excitatory cortical inputs to pallidal neurons via the subthalamic nucleus in the monkey. J. Neurophysiol. 84 (1), 289–300.
Neely, K.A., Kurani, A.S., Shukla, P., Planetta, P.J., Wagle Shukla, A., Goldman, J.G., et al., 2014. Functional brain activity relates to 0-3 and 3-8 Hz force oscillations in essential tremor. Cereb. Cortex 25 (11), 4191–4202.
Neely, K.A., Kurani, A.S., Shukla, P., Planetta, P.J., Wagle Shukla, A., Goldman, J.G., et al., 2015. Functional brain activity relates to 0-3 and 3-8 Hz force oscillations in essential tremor. Cereb. Cortex 25 (11), 4191–4202.
Oswal, A., Beudel, M., Zrinzo, L., Limousin, P., Hariz, M., Foltynie, T., et al., 2016. Deep brain stimulation modulates synchrony within spatially and spectrally distinct resting state networks in Parkinson's disease. Brain 139, 1482–1496 Pt 5.
Priori, A., Lefaucheur, J.P., 2007. Chronic epidural motor cortical stimulation for movement disorders. Lancet Neurol. 6 (3), 279–286.
Reich, M.M., Brumberg, J., Pozzi, N.G., Marotta, G., Roothans, J., Astrom, M., et al., 2016. Progressive gait ataxia following deep brain stimulation for essential tremor: adverse effect or lack of efficacy. Brain 139 (11), 2948–2956.
Rogasch, N.C., Daskalakis, Z.J., Fitzgerald, P.B., 2013. Mechanisms underlying long-interval cortical inhibition in the human motor cortex: a TMS-EEG study. J. Neurophysiol. 109 (1), 89–98.
Sammartino, F., Krishna, V., King, N.K., Lozano, A.M., Schwartz, M.L., Huang, Y., et al., 2016. Tractography-based ventral intermediate nucleus targeting: novel methodology and intraoperative validation. Mov. Disord. 31 (8), 1217–1225.
Schnitzler, A., Munks, C., Butz, M., Timmermann, L., Gross, J., 2009. Synchronized brain network associated with essential tremor as revealed by magnetoencephalography. Mov. Disord. 24 (11), 1629–1635.
Sharifi, S., Nederveen, A.J., Booij, J., van Rootselaar, A.F., 2014. Neuroimaging essentials in essential tremor: a systematic review. NeuroImage Clin. 5, 217–231.
Taulu, S., Simola, J., 2006. Spatiotemporal signal space separation method for rejecting nearby interference in MEG measurements. Phys. Med. Biol. 51 (7), 1759–1768.
Thobois, S., Hotton, G.R., Pinto, S., Wilkinson, L., Limousin-Dowsey, P., Brooks, D.J., et al., 2007. STN stimulation alters pallidal-frontal coupling during response selection under competition. J. Cereb. Blood Flow Metab. 27 (6), 1173–1184.
Udupa, K., Bahl, N., Ni, Z., Gunraj, C., Mazzella, F., Moro, E., et al., 2016. Cortical plasticity induction by pairing subthalamic nucleus deep-brain stimulation and primary motor cortical transcranial magnetic stimulation in Parkinson's disease. J. Neurosci. 36 (2), 396–404.
Walker, H.C., Huang, H., Gonzalez, C.L., Bryant, J.E., Killen, J., Cutter, G.R., et al., 2012a. Short latency activation of cortex during clinically effective subthalamic deep brain stimulation for Parkinson's disease. Mov. Disord. 27 (7), 864–873.
Walker, H.C., Huang, H., Gonzalez, C.L., Bryant, J.E., Killen, J., Knowlton, R.C., et al., 2012b. Short latency activation of cortex by clinically effective thalamic brain stimulation for tremor. Mov. Disord. 27 (11), 1404–1412.
Whitmer, D., de Solages, C., Hill, B., Yu, H., Henderson, J.M., Bronte-Stewart, H., 2012. High frequency deep brain stimulation attenuates subthalamic and cortical rhythms in Parkinson's disease. Front. Hum. Neurosci. 6, 155.